Effect of lateral electric field on the transition energies of neutral and charged excitons in $In_{0.5}Ga_{0.5}As/GaAs$ quantum dots

Toshio Saito,[1] Toshihiro Nakaoka,[1,2] and Yasuhiko Arakawa[1]

[1]*Institute for Nano Quantum Information Electronics, The University of Tokyo, 4-6-1 Komaba, Meguro-ku, Tokyo 153-8505, Japan*

[2]*Faculty of Science and Technology, Sophia University, 7-1 Kioi, Chiyoda-ku, Tokyo 102-8554, Japan*

(Received 2 May 2013; revised manuscript received 23 January 2015; published 12 March 2015)

We have calculated the transition energies of neutral and charged excitons in $In_{0.5}Ga_{0.5}As/GaAs$ quantum dots (QDs) under a lateral electric field up to 40 kV/cm. First, the single-particle electron and hole states under the lateral field are calculated using the 8-band $\mathbf{k}\cdot\mathbf{p}$ theory. The linear and quadratic piezoelectricity is included. Next, the transition energies are calculated from the electron-hole, electron-electron, and hole-hole Coulomb energies. For a QD with 15-nm base length under a lateral electric field along the [100] direction, the transition energy of the positively charged exciton exhibits a blueshift with increasing field up to 28 kV/cm, followed by a redshift under higher field. In contrast, those of the neutral and negatively charged excitons exhibit only redshifts accompanied by a crossing of the two exciton levels. The calculated result for the positively charged exciton reproduces the unconventional "M"-shaped exciton energy shift observed in our experiment by Nakaoka *et al.* [Appl. Phys. Lett. **99**, 181109 (2011)]. The origin of the blueshift calculated for the positively charged exciton is the enhanced hole density in the QD base corner due to the modification of the piezoelectric potential by the lateral electric field, which causes an increase in the hole-hole Coulomb energy. We found that the amount of the blueshift increases with the QD size. In order to understand the effect of the lateral field direction, we calculate the transition energies under a lateral electric field of 20 kV/cm along the $[1\bar{1}0]$, [100], and [110] directions. For the positively charged exciton, the transition energy exhibits a redshift for the $[1\bar{1}0]$ direction, and blueshifts of different amounts for the [100] and [110] directions, indicating that the effects of the lateral field are not equivalent for the $[1\bar{1}0]$ and [110] directions. It is demonstrated that the direction dependence of the transition energy reflects the symmetry of the confinement potential in the QDs due to piezoelectricity.

DOI: 10.1103/PhysRevB.91.115306 PACS number(s): 78.67.−n, 73.21.La, 71.35.−y

I. INTRODUCTION

Electronic and optical properties of semiconductor quantum dots (QDs) have attracted researchers' attentions because of their atomic-like properties of electronic states: zero-dimensionally confined electron and hole states with discrete energy levels [1]. Their investigations have concentrated on the optical transitions from excitons and their complexes which are formed by the Coulomb interactions between electrons and holes. Control of these excitonic transitions are important to realize quantum information devices such as single-photon emitters and entangled photon pair generators [2]. The control of the excitonic transitions has been investigated by applying external fields: electric, magnetic, and strain fields [3–5].

As a device-compatible method, application of an electric field through gate electrodes has been investigated for control. At first, the effects of a vertical electric field along the [001] direction on photoluminescence (PL) from InAs/GaAs QD samples were studied [3]. It was found that the PL transition energies decrease with increasing magnitude of the electric field for both positive and negative field directions: i.e., the Stark redshift [3]. The maxima of the transition energies occur at nonzero electric fields [3]. The transition energies show asymmetric change with respect to the zero field. Some theoretical calculations for the transition energies were performed using an 8-band $\mathbf{k}\cdot\mathbf{p}$ theory [6,7]. The calculated transition energies show asymmetric change depending on the vertical alignment of electron and hole wave functions which reflect asymmetry of the QD shape, pyramids or truncated pyramids, along the vertical direction.

The effects of lateral electric fields were studied by fabricating gate electrodes near the QD structures [8–10]. It is expected that transition energies will show symmetric change when the vertical component of the field is zero. However, the typical PL data show asymmetric change with the lateral applied bias, implying nonzero vertical component [8].

On the other hand, we recently succeeded in observing symmetric change in transition energies under a lateral electric field using a side-gate device [11]. Our PL transition energies show, for both positive and negative biases along the [100] direction, (i) a redshift with a lateral bias, or (ii) a blueshift with a lower bias followed by a redshift with a higher bias ("M"-shaped shift) [11]. We briefly showed calculated transition energy shifts of neutral and charged excitons, which were obtained from the electron and hole Coulomb energies [11]. The 8-band $\mathbf{k}\cdot\mathbf{p}$ theory [12] was used for calculation of single-particle electron and hole states. It was found that only the positively charged exciton shows the M-shaped shift.

In addition to the above calculations, further studies are required to understand the effect of the lateral field more completely. First, the effects of the lateral field on the order of transition energies, ω, should be clarified. The most typical order is $\omega(X^-) < \omega(X^0) < \omega(X^+)$ under zero field [13]; here X^0 is a neutral exciton and X^+ (X^-) is a positively (negatively) charged exciton. However, the order may change under the lateral field depending on the size and position of electron and hole wave functions. In some lateral fields, a crossing of the exciton levels may occur. Second, the changes of electron and hole wave functions under lateral fields should be understood more properly considering the piezoelectric potential in the

QDs. Third, the dependence of the lateral field *direction* on the optical transitions should be presented, because only the [100] direction was examined in our previous study [11]. Can we tune the optical transitions by varying the lateral field direction, for example, to $[1\bar{1}0]$ and [110]?

So far, some theoretical calculations of excitonic states in QDs under a lateral field have been reported [14,15]. In these studies, the lateral confinement of the QDs has been treated as a two-dimensional harmonic potential [14,15]. No one has calculated QD excitonic states under a lateral field based on a realistic QD shape accompanied with strain and piezoelectric potential.

In the present paper, in order to answer the above three issues, we perform detailed and extended calculations for transition energies of neutral and charged excitons in $In_{0.5}Ga_{0.5}As$/GaAs QDs under lateral electric fields. First, the single-particle electron and hole states under the lateral field are calculated using the 8-band $\mathbf{k}\cdot\mathbf{p}$ theory [12]. The linear and quadratic piezoelectricity is included [16,17]. Next, the transition energies are calculated from the electron-hole, electron-electron, and hole-hole Coulomb energies. Methods of calculation are described in Sec. II. In Sec. III, we show the transition energies under a lateral electric field along the [100] direction, E[100], up to 40 kV/cm. The QD base lengths, b, are 12.5, 15, and 20 nm. In Sec. IV, we show the dependence of the excitonic states on the lateral electric field directions, $[1\bar{1}0]$, [100], and [110], under the constant magnitude of the field $|\mathbf{E}| = 20$ kV/cm. The conclusions are summarized in Sec. V.

II. METHODS OF CALCULATION

We calculate the transition energies (ω) of a neutral exciton (X^0) and positively and negatively charged excitons (X^+, X^-) in $In_{0.5}Ga_{0.5}As$/GaAs QDs under lateral electric fields using the methods as described in the steps (i)–(v) below.

(i) We set up a QD model for the calculations. Here we adopt a pyramidal $In_{0.5}Ga_{0.5}As$ QD embedded in a GaAs barrier layer, as shown in Fig. 1(a). The pyramidal QD has a (001) base plane and {101} facets. The base edges are oriented to the [100] and [010] directions. The base length b (height h) of the QD is chosen as 12.5 nm (6.25 nm), 15 nm (7.5 nm), and 20 nm (10 nm).

(ii) For the QD model, we calculate distribution of strain, ϵ_{ij} (here $i,j = x,y,z$), arising from the difference in the lattice constants between $In_{0.5}Ga_{0.5}As$ and GaAs. We use a linear static analysis based on the elastic continuum theory [18].

(iii) We calculate the piezoelectric potential, $V_p(\mathbf{r})$, from the strain distribution obtained in (ii). First, the piezoelectric polarization, $\mathbf{P}$, is calculated as

$$\mathbf{P} = \mathbf{P}_1 + \mathbf{P}_2. \tag{1}$$

Here $\mathbf{P}_1$ and $\mathbf{P}_2$ are the linear and quadratic piezoelectric polarizations, respectively, expressed as [16,17]

$$\mathbf{P}_1 = 2e_{14}\begin{pmatrix}\epsilon_{yz}\\ \epsilon_{xz}\\ \epsilon_{xy}\end{pmatrix} \tag{2}$$

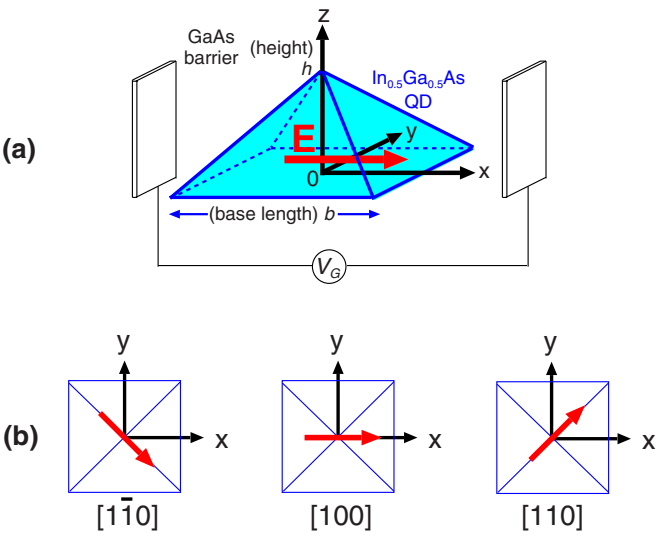

FIG. 1. (Color online) Model structure of a pyramidal $In_{0.5}Ga_{0.5}As$/GaAs quantum dot: (a) an oblique view showing a lateral electric field, $\mathbf{E}$, applied by the two electrodes, and (b) top views showing directions of the lateral electric fields, $[1\bar{1}0]$, [100], and [110], from left to right. The quantum dot base is at $z = 0$, and the top is at $z = h$.

and

$$\mathbf{P}_2 = 2B_{114}\begin{pmatrix}\epsilon_{xx}\epsilon_{yz}\\ \epsilon_{yy}\epsilon_{xz}\\ \epsilon_{zz}\epsilon_{xy}\end{pmatrix} + 2B_{124}\begin{pmatrix}\epsilon_{yz}(\epsilon_{yy}+\epsilon_{zz})\\ \epsilon_{xz}(\epsilon_{zz}+\epsilon_{xx})\\ \epsilon_{xy}(\epsilon_{xx}+\epsilon_{yy})\end{pmatrix} + 4B_{156}\begin{pmatrix}\epsilon_{xz}\epsilon_{xy}\\ \epsilon_{yz}\epsilon_{xy}\\ \epsilon_{yz}\epsilon_{xz}\end{pmatrix}. \tag{3}$$

e_{14} is a piezoelectric constant for the linear case, and B_{114}, B_{124}, and B_{156} are those for the quadratic case [16,17]. Next, the piezoelectric charge, ρ_p, is calculated as $\rho_p = -\,\mathrm{div}\,\mathbf{P}$. Lastly, $V_p(\mathbf{r})$ is obtained as [19]

$$V_p(\mathbf{r}) = \frac{1}{4\pi\varepsilon_0\varepsilon_r}\int\frac{\rho_p(\mathbf{r}')}{|\mathbf{r}-\mathbf{r}'|}d^3\mathbf{r}'. \tag{4}$$

Here ε_0 is the permittivity of vacuum, and ε_r is the dielectric constant. For InAs (GaAs), we used e_{14}=−0.115 (−0.230) C/m^2, B_{114}=−0.531 (−0.439) C/m^2, $B_{124} = -4.076\,(-3.765)$ C/m^2, and $B_{156} = -0.120$ (−0.492) C/m^2, from Ref. [17]; $\varepsilon_r = 15.15\,(13.18)$. For the values of the parameters of $In_{0.5}Ga_{0.5}As$ QDs, the arithmetic means of the corresponding InAs and GaAs values were used.

(iv) We perform single-particle calculations of electron (e) and hole (h) states using the strain-dependent 8-band $\mathbf{k}\cdot\mathbf{p}$ theory formulated by Bahder [12] under an external electric field, $\mathbf{E}$. In the 8-band $\mathbf{k}\cdot\mathbf{p}$ theory, electron and hole wave functions in a QD, $\Psi(\mathbf{r})$, are expressed as [20,21]

$$\Psi(\mathbf{r}) = \sum_{j=1}^{8} F_j(\mathbf{r})|u_j\rangle; \tag{5}$$

here $F_j(\mathbf{r})$ is the envelope function, and $|u_j\rangle$ is the zone-center Bloch function for electron, heavy-hole, light-hole, and split-

off hole states. The envelope function, $F_j(\mathbf{r})$, is obtained by solving the equation

$$(H_{\mathbf{k}\cdot\mathbf{p}} + V_p + V_{\text{Stark}})\mathbf{F} = \epsilon\mathbf{F}, \tag{6}$$

where $H_{\mathbf{k}\cdot\mathbf{p}}$ is the strain-dependent 8-band $\mathbf{k}\cdot\mathbf{p}$ Hamiltonian [12], V_p is the piezoelectric potential obtained in the step (iii), V_{Stark} represents the potential induced by the applied electric field $\mathbf{E}$ as $V_{\text{Stark}} = e\mathbf{E}\cdot\mathbf{r}$ (e is the electronic charge), and ϵ is the eigenvalue. $\mathbf{F}$ is expressed as [22]

$$\mathbf{F} = [F_1(\mathbf{r}), F_2(\mathbf{r}), \ldots, F_8(\mathbf{r})]. \tag{7}$$

The material parameters for the $\mathbf{k}\cdot\mathbf{p}$ calculations are adopted from Ref. [18]. We used a finite-difference method to solve Eq. (6) numerically.

The directions of the lateral electric field, $\mathbf{E}$, examined in this study are $[1\bar{1}0]$, [100], and [110], as shown in Fig. 1(b).

(v) We calculate transition energies of neutral, positively charged, and negatively charged excitons [$\omega(X^0)$, $\omega(X^+)$, and $\omega(X^-)$, respectively] using the equations [13]

$$\omega(X^0) = e_0 - h_0 + J(e_0h_0), \tag{8}$$

$$\begin{aligned}\omega(X^+) &= (e_0 - h_0) + 2J(e_0h_0) + J(h_0h_0)\\ &= \omega(X^0) + J(e_0h_0) + J(h_0h_0),\end{aligned} \tag{9}$$

$$\begin{aligned}\omega(X^-) &= (e_0 - h_0) + 2J(e_0h_0) + J(e_0e_0)\\ &= \omega(X^0) + J(e_0h_0) + J(e_0e_0).\end{aligned} \tag{10}$$

Here e_0 and h_0 are ground-state energies of the electron and hole, respectively. $J(e_0h_0)$, $J(h_0h_0)$, and $J(e_0e_0)$ are electron-hole, hole-hole, and electron-electron Coulomb energies, respectively, which are calculated as

$$J(e_0h_0) = -e^2\int\int \frac{|\Psi_{e_0}(\mathbf{r}_1)|^2|\Psi_{h_0}(\mathbf{r}_2)|^2}{4\pi\varepsilon_0\varepsilon_r|\mathbf{r}_1-\mathbf{r}_2|}d^3\mathbf{r}_1d^3\mathbf{r}_2, \tag{11}$$

$$J(h_0h_0) = e^2\int\int \frac{|\Psi_{h_0}(\mathbf{r}_1)|^2|\Psi_{h_0}(\mathbf{r}_2)|^2}{4\pi\varepsilon_0\varepsilon_r|\mathbf{r}_1-\mathbf{r}_2|}d^3\mathbf{r}_1d^3\mathbf{r}_2, \tag{12}$$

$$J(e_0e_0) = e^2\int\int \frac{|\Psi_{e_0}(\mathbf{r}_1)|^2|\Psi_{e_0}(\mathbf{r}_2)|^2}{4\pi\varepsilon_0\varepsilon_r|\mathbf{r}_1-\mathbf{r}_2|}d^3\mathbf{r}_1d^3\mathbf{r}_2. \tag{13}$$

Here Ψ_{e_0} and Ψ_{h_0} are ground-state electron and hole wave functions, respectively. In the above definitions, we have $J(e_0h_0) < 0$, $J(h_0h_0) > 0$, and $J(e_0e_0) > 0$. Another set of definitions using opposite signs for the Coulomb energies, $J(e_0h_0) > 0$, $J(h_0h_0) < 0$, and $J(e_0e_0) < 0$, was adopted in Ref. [23]; here $J(e_0h_0)$ becomes identical to the exciton binding energy. In the present paper, we adopt the definitions of Eqs. (11)–(13) whose signs indicate that $J(e_0h_0)$ is an attractive interaction, and $J(h_0h_0)$ and $J(e_0e_0)$ are repulsive interactions.

The binding energies of positively charged and negatively charged excitons, $\Delta_{\text{bind}}(X^+)$ and $\Delta_{\text{bind}}(X^-)$, are defined as $\Delta_{\text{bind}}(X^+) = \omega(X^0) - \omega(X^+)$ and $\Delta_{\text{bind}}(X^-) = \omega(X^0) - \omega(X^-)$, respectively [13]. Each charged exciton is called *binding* (*antibinding*) when $\Delta_{\text{bind}} > 0$ ($\Delta_{\text{bind}} < 0$) [13].

In Eqs. (8)–(10), the transition energies ω are expressed, in the first order, in terms of the ground-state energies of the electron and hole, e_0 and h_0, respectively, and the Coulomb energies $J(e_0h_0)$, $J(h_0h_0)$, and $J(e_0e_0)$. The higher-order correction due to correlation effects and that due to exchange effects (as described in Ref. [13]) are omitted in the present paper. The magnitude of the correlation correction depends on the type of multiexcitons. A remarkable consequence is the change in order of neutral exciton and biexciton transition energies, $\omega(X^0)$ and $\omega(XX^0)$, respectively [13]. Hence we exclude $\omega(XX^0)$ in the present calculation. The exchange correction is very small compared to the Coulomb energies and correlation correction [13]. To account for the higher-order corrections, the configuration interaction (CI) method is required [13]. The absorption spectra of neutral and charged excitons can be calculated using the CI method combined with Fermi's golden rule [17]. The peaks of the spectra are broadened by typically ≈10 meV width for comparison to experimental results, while each peak area corresponds to the oscillator strength [24].

III. TRANSITION ENERGIES UNDER THE LATERAL ELECTRIC FIELD: E ∥ [100]

A. QD of medium size: $b = 15$ nm

First we show the results of calculations for the QD with a base length b of 15 nm under the lateral electric field $\mathbf{E}$ along the [100] direction, denoted by $E[100]$, corresponding to the [100] case of Fig. 1(b). Figure 2(a) shows the single-particle energy difference $(e_0 - h_0)$ and Coulomb energies $[J(e_0h_0), J(h_0h_0), J(e_0e_0)]$ as a function of $E[100]$ up to 40 kV/cm. The energy difference $(e_0 - h_0)$ decreases with increasing $E[100]$. This redshift is nothing but the quantum-confined Stark effect, QCSE, due to the lateral electric field. At the same time, the magnitude of $J(e_0h_0)$, $|J(e_0h_0)| = -J(e_0h_0)$, decreases with increasing $E[100]$. This generally indicates that the hole wave function Ψ_{h_0} moves along the lateral electric field, while the electron wave function Ψ_{e_0} moves along the opposite direction, and hence $|J(e_0h_0)|$ decreases due to the reduction of overlap between the two wave functions. Figure 2(a) also shows that, with increasing $E[100]$, $J(h_0h_0)$ increases remarkably, while $J(e_0e_0)$ changes very little, indicating that the extent of the hole wave function becomes much smaller, but that of the electron wave function changes very little. The difference in changes between electron and hole is caused by the difference in the effective mass of the two.

The difference in changes of the electron and hole wave functions with $E[100]$ suggested above is confirmed directly by plotting the electron and hole envelope functions, as shown later in Sec. IV. The discussion is given considering the effect of the piezoelectricity in the same section.

Figure 2(b) shows the calculated transition energies [$\omega(X^0)$, $\omega(X^+)$, and $\omega(X^-)$] as a function of $E[100]$, which are obtained from Eqs. (8)–(10). For $E[100] = 0$ kV/cm, ordering of the transition energies is $\omega(X^-) < \omega(X^0) < \omega(X^+)$. This ordering is considered as the prototype one in InAs/GaAs QDs, resulting from the ordering of the Coulomb energies $J(e_0e_0) < |J(e_0h_0)| < J(h_0h_0)$, as described in Ref. [13]. Our calculated Coulomb energies in Fig. 2(a) show this ordering for $E[100] = 0$ kV/cm. The above ordering of the Coulomb energies indicates that the extent of the electron wave function Ψ_{e_0} is larger than that of the hole wave function Ψ_{h_0}, and Ψ_{h_0} is

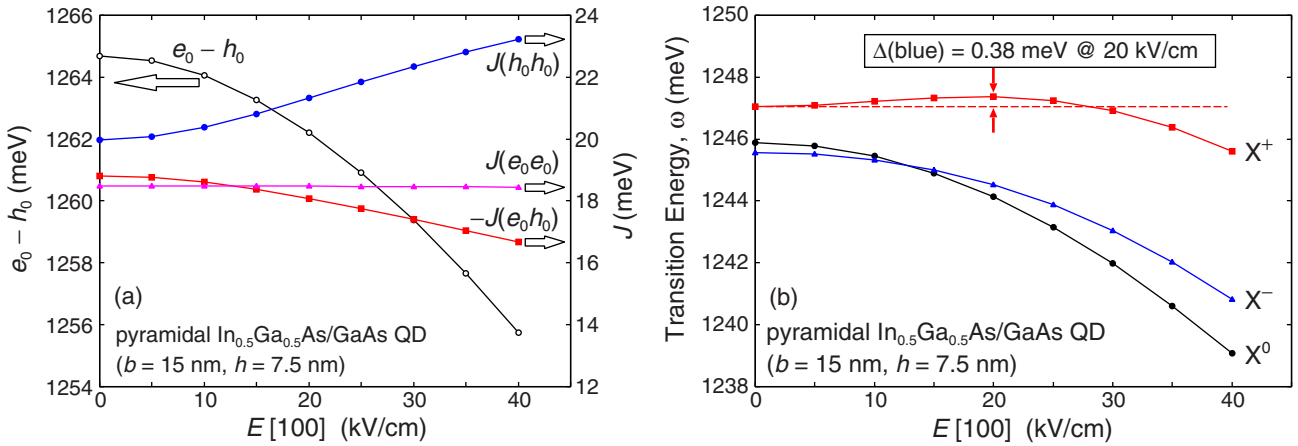

FIG. 2. (Color online) Effects of the lateral electric field **E** along the [100] direction, $E[100]$, on (a) the single-particle energy difference $(e_0 - h_0)$ and electron-hole, hole-hole, and electron-electron Coulomb energies [$J(e_0h_0)$, $J(h_0h_0)$, and $J(e_0e_0)$, respectively], and (b) the transition energies, ω, for the neutral exciton (X^0) and positively and negatively charged excitons (X^+ and X^-, respectively), in the pyramidal $In_{0.5}Ga_{0.5}As$/GaAs quantum dot. The base length b is 15 nm. In (a), the left vertical axis is for $e_0 - h_0$, and the right one is for J's. Note that the sign is reversed for $J(e_0h_0)$.

mostly enclosed in Ψ_{e_0} [13]. This is confirmed later in Fig. 6. We believe that the conclusions of the present study are of interest for other groups in the field, since our QD structure is not an extremely specific one but a prototype.

With increasing $E[100]$, the transition energies of neutral and negatively charged excitons, $\omega(X^0)$ and $\omega(X^-)$, respectively, exhibit only redshifts; i.e., the usual QCSE. At the same time, we find that the lines of $\omega(X^0)$ and $\omega(X^-)$ cross each other at $E[100] = 13$ kV/cm. At this field magnitude, the ordering changes from $\omega(X^-) < \omega(X^0)$ to $\omega(X^0) < \omega(X^-)$, and the negatively charged exciton changes from binding $[\Delta_{\rm bind}(X^-) > 0]$ to antibinding $[\Delta_{\rm bind}(X^-) < 0]$, as defined in Sec. II. This is a consequence of the change in ordering from $J(e_0e_0) < |J(e_0h_0)|$ to $|J(e_0h_0)| < J(e_0e_0)$ at $E[100] = 13$ kV/cm [see Fig. 2(a)], because the binding energy is expressed from Eq. (10) as, $\Delta_{\rm bind}(X^-) = \omega(X^0) - \omega(X^-) = -J(e_0h_0) - J(e_0e_0) = |J(e_0h_0)| - J(e_0e_0)$. Here the decrease of $|J(e_0h_0)|$ with $E[100]$ plays a major role in the binding-antibindig change of X^-, because the change of $J(e_0e_0)$ is very small as described before.

On the other hand, the transition energy of positively charged exciton, $\omega(X^+)$, exhibits a blueshift with increasing $E[100]$ up to 28 kV/cm, i.e., $\Delta\omega(X^+) \equiv \omega(X^+) - \omega^0(X^+) > 0$; here the superscrpit "0" refers to the corresponding value at $E[100] = 0$. The maximum blueshift, Δ(blue), is 0.38 meV at $E[100] = 20$ kV/cm. Furthermore this blueshift is followed by a redshift, $\Delta\omega(X^+) < 0$, under the higher $E[100]$. The origin of the blueshift is understood by the expression of $\Delta\omega(X^+)$ deduced from Eq. (9) as

$$\Delta\omega(X^+) = \omega(X^+) - \omega^0(X^+) = \Delta(e_0 - h_0) + 2\Delta J(e_0h_0) + \Delta J(h_0h_0); \quad (14)$$

here $\Delta(e_0 - h_0) = (e_0 - h_0) - (e^0_0 - h^0_0)$, $\Delta J(e_0h_0) = J(e_0h_0) - J^0(e_0h_0)$, and $\Delta J(h_0h_0) = J(h_0h_0) - J^0(h_0h_0)$. The superscript "0" refers to the corresponding value at $E[100] = 0$ kV/cm again. As shown in Fig. 2(a), we find $\Delta(e_0 - h_0) < 0$ (redshift contribution), but $\Delta J(e_0h_0) > 0$ and $\Delta J(h_0h_0) > 0$ (blueshift contribution). The sign of $\Delta\omega(X^+)$ is determined by the competition between the redshift and blueshift contributions. Up to $E[100] = 28$ kV/cm, the latter contribution overcomes the former one resulting in $\Delta\omega(X^+) > 0$. However, at $E[100] > 28$ kV/cm, the former overcomes the latter resulting in $\Delta\omega(X^+) < 0$ because of the faster decrease of $(e_0 - h_0)$. Since Eq. (14) is valid not only for our samples but also for any samples of other groups, one might expect a blueshift for the quantum confined Stark effect under the condition that the blueshift contribution overcomes the redshift one.

For the negatively charged exciton, the similar relation holds as

$$\Delta\omega(X^-) = \omega(X^-) - \omega^0(X^-) = \Delta(e_0 - h_0) + 2\Delta J(e_0h_0) + \Delta J(e_0e_0); \quad (15)$$

here $\Delta J(e_0e_0) = J(e_0e_0) - J^0(e_0e_0)$. Since $\Delta J(e_0e_0) \approx 0$ [see Fig. 2(a)], the redshift contribution, $\Delta(e_o - h_0)$, always overcomes the blueshift one, $\Delta J(e_0h_0)$, resulting in $\Delta\omega(X^-) < 0$. Considering that the $\Delta J(h_0h_0)$ term in Eq. (14) is replaced by $\Delta J(e_0e_0)$ in Eq. (15), the large value of $\Delta J(h_0h_0)$, or the remarkable increase in $J(h_0h_0)$ with $E[100]$, causes the blueshift of $\omega(X^+)$ at $E[100] < 28$ kV/cm. The remarkable increase in $J(h_0h_0)$ is a result of the smaller extent of the hole wave function, Ψ_{h_0}, as stated before.

For a QD of medium size ($b = 15$ nm), we predict that (i) the transition energy of the negatively charged exciton $\omega(X^-)$ shows the binding-antibinding change at $E[100] = 13$ kV/cm, and (ii) that of the positively charged exciton $\omega(X^+)$ shows a blueshift at $E[100] < 28$ kV/cm, followed by a redshift at $E[100] > 28$ kV/cm.

B. QDs of smaller and larger sizes: $b = 12.5$ nm and 20 nm

Figure 3 shows the calculated transition energies [$\omega(X^0)$, $\omega(X^+)$, and $\omega(X^-)$] as a function of $E[100]$ for the QDs with (a) $b = 12.5$ nm and (b) $b = 20$ nm. For $b = 12.5$ nm, the ordering of the transition energies at $E[100] = 0$ kV/cm is $\omega(X^-) < \omega(X^0) < \omega(X^+)$, which is the same prototype ordering as that for $b = 15$ nm. With increasing $E[100]$,

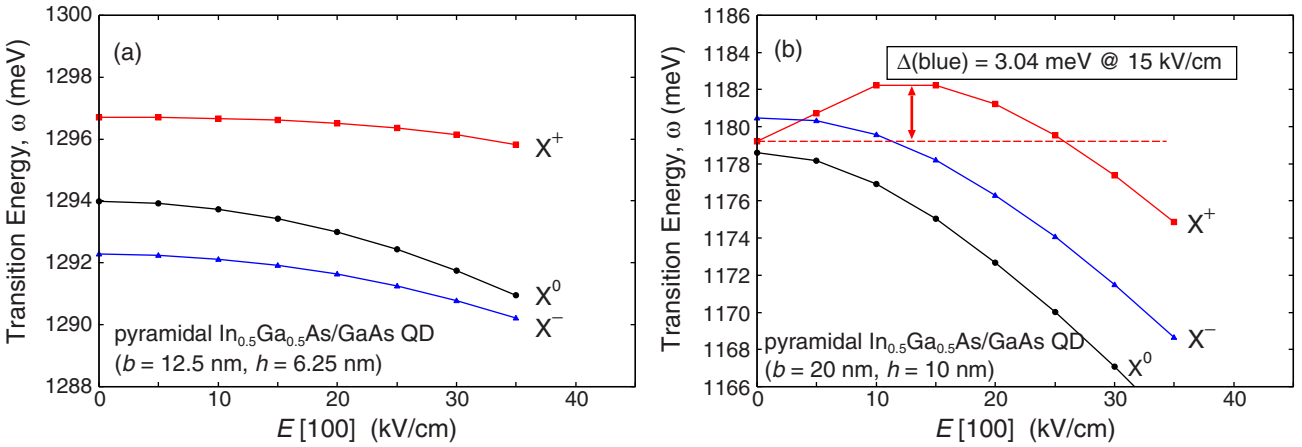

FIG. 3. (Color online) Effects of the lateral electric field **E** along the [100] direction, $E[100]$, on the transition energies ω for the neutral exciton (X^0) and positively and negatively charged excitons (X^+ and X^-, respectively) in pyramidal $In_{0.5}Ga_{0.5}As/GaAs$ quantum dots; here the base length b is (a) 12.5 nm and (b) 20 nm.

$\omega(X^0)$ and $\omega(X^-)$ exhibit redshifts with no line crossing up to $E[100] = 35\,\mathrm{kV/cm}$. $\omega(X^+)$ also exhibits a redshift in contrast with the blueshift followed by the redshift for $b = 15$ nm. For $b = 12.5$ nm, the effect of $E[100]$ is weaker, and no unsual change in ω, such as a blueshift, occurs.

For $b = 20$ nm, the ordering of the transition energies at $E[100] = 0$ kV/cm is $\omega(X^0) < \omega(X^+) < \omega(X^-)$ showing that X^+ and X^- are antibinding. This ordering results from that of our calculated Coulomb energies $|J(e_0h_0)| < J(h_0h_0) < J(e_0e_0)$. This is the case for large pyramidal QDs with a large internal piezoelectric field [13]. With increasing $E[100]$, $\omega(X^0)$ and $\omega(X^-)$ exhibit redshifts. In contrast, $\omega(X^+)$ exhibits a blueshift up to 26 kV/cm, followed by a redshift under the higher $E[100]$. The maximum blueshift, Δ(blue), is 3.04 meV which is about one order of magnitude larger than the corresponding value for $b = 15$ nm. As for $b = 15$ nm, the remarkable increase in $J(h_0h_0)$ causes the blueshift. The increase in $J(h_0h_0)$ is larger for larger QDs, resulting in the larger maximum blueshift, as seen in Fig. 3(b).

As shown in Figs. 2(b) and 3(b), we find that the ordering of the exciton transition energies for $E[100] = 0$ kV/cm is $\omega(X^-) < \omega(X^0) < \omega(X^+)$ for the pyramidal QD of medium size ($b = 15$ nm), and $\omega(X^0) < \omega(X^+) < \omega(X^-)$ for that of a larger size ($b = 20$ nm). With increasing $E[100]$, the ordering eventually changes to $\omega(X^0) < \omega(X^-) < \omega(X^+)$ for both sizes. For the pyramidal QDs, we do not find the ordering, $\omega(X^+) < \omega(X^0) < \omega(X^-)$, since this ordering is expected for QDs with a large vertical aspect ratio as mentioned in Ref. [13]. *(The possible ordering is limited to the above four types also as mentioned in Ref. [13].)* In summary, it is possible to achieve control of the ordering not only by sample preparation but also by application of an electric field.

C. Comparison with our experiments

In this subsection, we compare the calculated transition energy for the positively charged exciton, $\omega(X^+)$, with our experimental PL peak energy [11] in order to find an

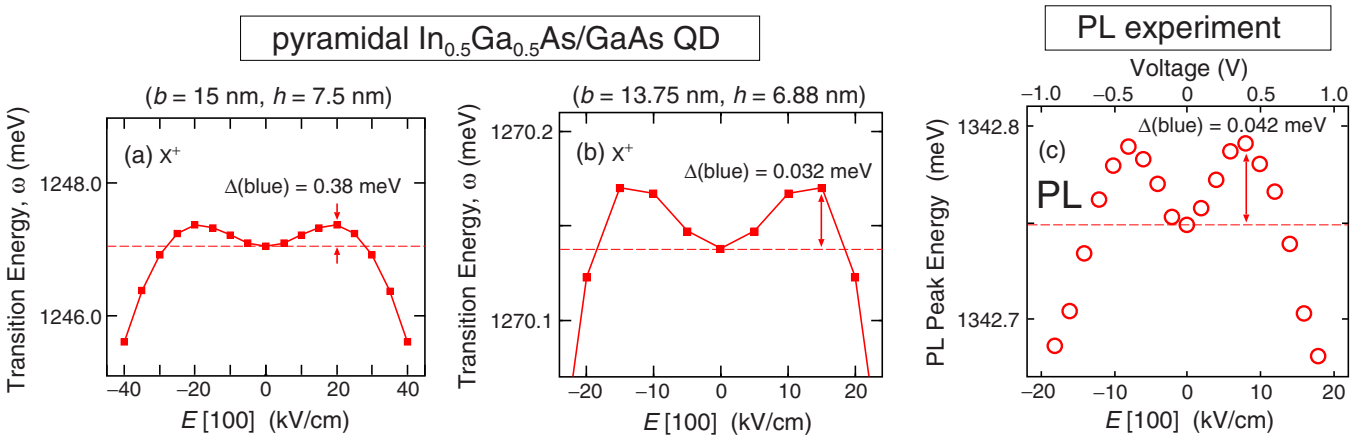

FIG. 4. (Color online) Calculated transition energy ω for the positively charged exciton X^+ in pyramidal $In_{0.5}Ga_{0.5}As/GaAs$ quantum dots as a function of *positive and negative* lateral electric fields **E** along the [100] direction, $E[100]$; here the base length b is (a) 15 nm and (b) 13.75 nm. Panel (c) shows the photoluminescence (PL) peak energy as a function of $E[100]$ in the $In_{0.5}Ga_{0.5}As$ quantum dot sample measured by Nakaoka *et al.* in Ref. [11]. The corresponding gate bias voltage is indicated by the upper horizontal axis in (c). The calculated ω in (a) and (b) and the PL peak energy in (c) show the M-shaped shift in energy.

appropriate QD size which can reproduce the observed PL blueshift.

In Figs. 4(a) and 4(b), we show the calculated $\omega(X^+)$ as a function of *positive and negative* E[100]; here the base length b is (a) 15 nm (the medium size QD) and (b) 13.75 nm. The latter b is the middle value between 15 nm (the medium size) and 12.5 nm (the smaller size). In (a), $\omega(X^+)$ for positive E[100] was already shown in Fig. 2(b). As seen in these figures, $\omega(X^+)$ exhibits symmetrical M-shaped shifts showing the blueshift followed by the redshift with increasing magnitude of E[100]. The maximum blueshift, Δ(blue), is 0.380 meV for $b = 15$ nm and 0.032 meV for $b = 13.75$ nm.

Figure 4(c) shows the PL peak energy as a function of E[100] in the self-assembled $In_{0.5}Ga_{0.5}As$ QD sample measured by us (Nakaoka *et al.* [11]). In the sample, the two gate electrodes are fabricated near the QDs so that the lateral electric field E[100] is applied to the QDs. The gate bias voltage of 1.0 V (−1.0 V), for example, induces E[100] = 20 kV/cm (−20 kV/cm) as clarified by the simulation of the field distribution [11] [(see Fig. 1(e) in Ref.[11]). The gate bias voltage corresponding to E[100] is indicated by the upper horizontal axis. The PL peak energy also exhibits an M-shaped shift with Δ(blue) = 0.042 meV, which suggests that the observed PL peak can be assigned to the unusual X^+ transition. The QD size of $b = 13.75$ nm [Δ(blue) = 0.032 meV] is appropriate to reproduce the observed PL blueshift [Δ(blue) = 0.042 meV].

The M-shaped curves in Fig. 4 are symmetric for *positive and negative* E[100]. This is a fundamental property arising from the condition that a lateral electric field *with no vertical component* is applied to a laterally symmetric QD because the transition energies show asymmetric change under a vertical electric field, as stated in Sec. I.

The calculated transition energy for $b = 13.75$ nm is smaller by ≈72 meV than the PL peak energy. To obtain more complete agreement between the calculated and PL energies, slight modification of other QD parameters, such as the In composition or the QD shape, is required.

IV. DEPENDENCE OF THE TRANSITION ENERGIES ON THE LATERAL ELECTRIC FIELD DIRECTION: E ∥ [1$\bar{1}$0], [100], and [110]

In this section, we show the calculated electron and hole envelope functions, Coulomb energies [$J(e_0h_0)$, $J(e_0e_0)$, and $J(h_0h_0)$,], and transition energies [$\omega(X^0)$, $\omega(X^+)$, and $\omega(X^-)$] under lateral electric fields **E** of three different directions: **E** ∥ [1$\bar{1}$0], [100], and [110]. The calculations are performed for the QD of medium size ($b = 15$ nm) keeping $|\mathbf{E}| = 20$ kV/cm, at which the blueshift of $\omega(X^+)$ has a maximum under E[100].

A. Piezoelectric potential and its modification by the lateral electric field

Figure 5 shows the piezoelectric potential, V_p, on a (001) plane at $z = 1.5$ nm; here the QD base is at $z = 0$ nm. Under $|\mathbf{E}| = 0$ kV/cm, V_p calculated with the linear piezoelectricity only [see Fig. 5(a)] has two maxima near the QD corners on the [110] diagonal and two minima near those on the [1$\bar{1}$0] diagonal, producing C_{2v} symmetry. For V_p calculated with the quadratic piezoelectricity only [see Fig. 5(b)], the sign of V_p is opposite and the absolute values of the two maxima and two minima are significantly smaller compared to V_p calculated with the linear piezoelectricity only. (Note that the potentials are displayed in different ranges as indicated in the caption.) As a result, the total V_p calculated with the linear and quadratic piezoelectricity [see Fig. 5(c)] is similar to that with the linear piezoelectricity only, where the linear contribution is canceled slightly (≈ 6 meV) by the quadratic one which has an opposite sign. *Finally, the total V_p is largely dominated by the linear piezoelectric contribution.*

The above result of the relative contribution of the linear and quadratic piezoelectricity in the pyramidal $In_{0.5}Ga_{0.5}As$/GaAs QD ($b = 15$ nm) is consistent with the previous calculations by Schliwa and coworkers [17]. They showed that, in the pyramidal InAs/GaAs QD with {101} facets ($b = 17.2$ nm), V_p is largely dominated by the quadratic piezoelectric contribution [17]. With increasing Ga content in the QD, the quadratic contribution rapidly decreases [17]. For the Ga content of 0.15, V_p inside the QD shows virtually no piezoelectric field since the linear and quadratic contributions cancel out [13]. As a result, for the pyramidal $In_{0.7}Ga_{0.3}As$/GaAs QD, V_p is dominated by the linear piezoelectric contribution [17]. In the present study for the pyramidal $In_{0.5}Ga_{0.5}As$/GaAs QD, the linear piezoelectric contribution becomes even more dominant by a further increase in the Ga content, as shown in Figs. 5(a)–5(c).

Figure 5(d) shows the sum, $V_p + V_{\text{Stark}}$, on the same (001) plane for **E** ∥ [100] and $|\mathbf{E}| = 20$ kV/cm; here $V_p + V_{\text{Stark}}$ expresses the total piezoelectric potential modified by the lateral electric field. In contrast with V_p in Fig. 5(c), inside the QD we find only one maximum near the [110] corner and only one minimum near the [$\bar{1}$10] corner in Fig. 5(d). This is because the energy at the maximum near the [110] corner increases, while that at the maximum near the [$\bar{1}\bar{1}$0] corner decreases due to the potential gradient caused by **E** ∥ [100]. The similar reason holds for the presence of only one V_p minimum.

B. Envelope functions calculated with the piezoelectricity

We calculate the squared envelope functions, $|\mathbf{F}|^2$, for the electron and hole in the QDs as $|\mathbf{F}|^2 = \sum_{j=1}^{8} |F_j(\mathbf{r})|^2$ using the solution **F** of Eq. (6). Figure 6 shows $|\mathbf{F}|^2$ on a (001) plane at $z = 1.5$ nm for the ground-state electron (e_0) and hole (h_0); here the QD base is at $z = 0$ nm. $|\mathbf{F}|^2$, or the electron and hole charge densities, under $|\mathbf{E}| = 0$ kV/cm and $|\mathbf{E}| = 20$ kV/cm with **E** ∥ [1$\bar{1}$0], [100], and [110] are compared.

Under $|\mathbf{E}| = 0$ kV/cm, $|\mathbf{F}|^2$ for h_0 shows an apparent elongation along [110], while that for e_0 shows a nearly circular distribution with an inappreciable elongation along [1$\bar{1}$0], as already reported in various literature; for example, Ref. [13]. $|\mathbf{F}|^2$ for h_0 has C_{2v} symmetry because the QD confining potential has C_{2v} symmetry due to the piezoelectric potential, V_p, as already shown in Fig. 5(c).

With **E** ∥ [1$\bar{1}$0], $|\mathbf{F}|^2$ for h_0 is deviated toward the QD corner in the [1$\bar{1}$0] direction by the [1$\bar{1}$0] field, but its extent does not change much. $|\mathbf{F}|^2$ has C_{1v} symmetry with the (110) symmetry plane.

With **E** ∥ [100], $|\mathbf{F}|^2$ for h_0 moves significantly toward the QD corner in the [110] direction, *not moving in the* [100]

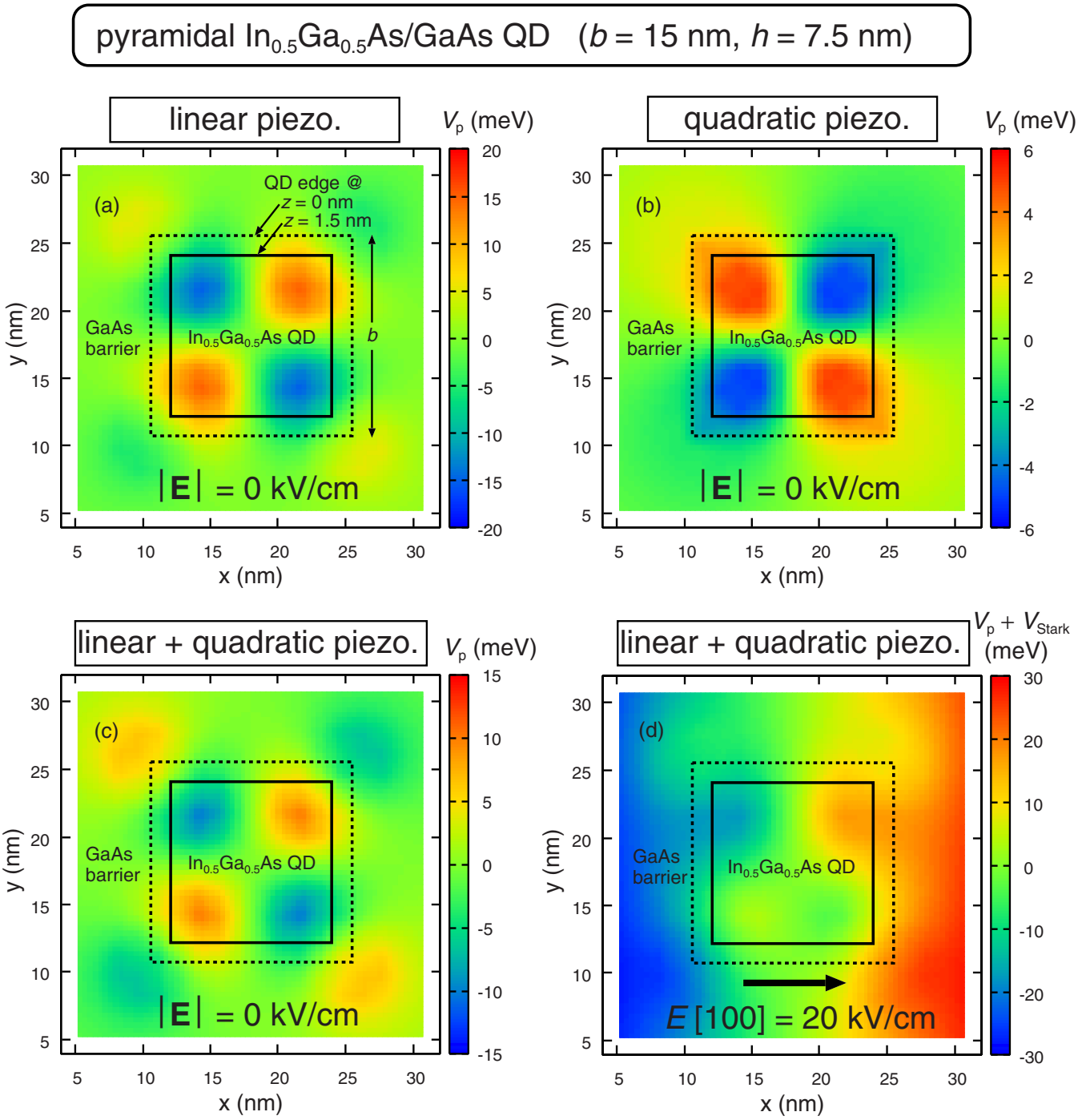

FIG. 5. (Color online) Piezoelectric potential, V_p, in the pyramidal $In_{0.5}Ga_{0.5}As/GaAs$ quantum dot (the base length $b = 15$ nm). V_p under $|\mathbf{E}| = 0$ kV/cm is calculated with (a) the linear piezoelectricity only, (b) the quadratic piezoelectricity only, and (c) the linear and quadratic piezoelectricity. Panel (d) shows the the sum of V_p in (c) and V_{Stark}; here V_{Stark} is the potential induced by the lateral electric field under $|\mathbf{E}| = 20$ kV/cm with $\mathbf{E} \parallel [100]$. In (a)–(d), the potentials on the (001) plane at $z = 1.5$ nm are displayed, here the quantum dot base is at $z = 0$ nm. Note that the potentials are displayed in the ranges of (a) -20 to 20 meV, (b) -6 to 6 meV, (c) -15 to 15 meV, and (d) -30 to 30 meV.

field direction, and its extent decreases remarkably. We also find that the $|\mathbf{F}|^2$ for h_0 is slightly asymmetric, having no symmetry plane. The origin of the seemingly unusual change in the $|\mathbf{F}|^2$ for h_0 is explained by considering $V_p + V_{\text{Stark}}$ which has one maximum and one minimum [see Fig. 5(d)]. With $\mathbf{E} \parallel [100]$, $|\mathbf{F}|^2$ of h_0 moves toward the maximum near the [110] corner, *not moving in the* [100] *field direction*, as shown in Fig. 6.

With $\mathbf{E} \parallel [110]$, $|\mathbf{F}|^2$ for h_0 moves more significantly toward the QD corner in the [110] direction, consistent with the field direction, and its extent decreases more remarkably. The $|\mathbf{F}|^2$ has C_{1v} symmetry with the $(1\bar{1}0)$ symmetry plane.

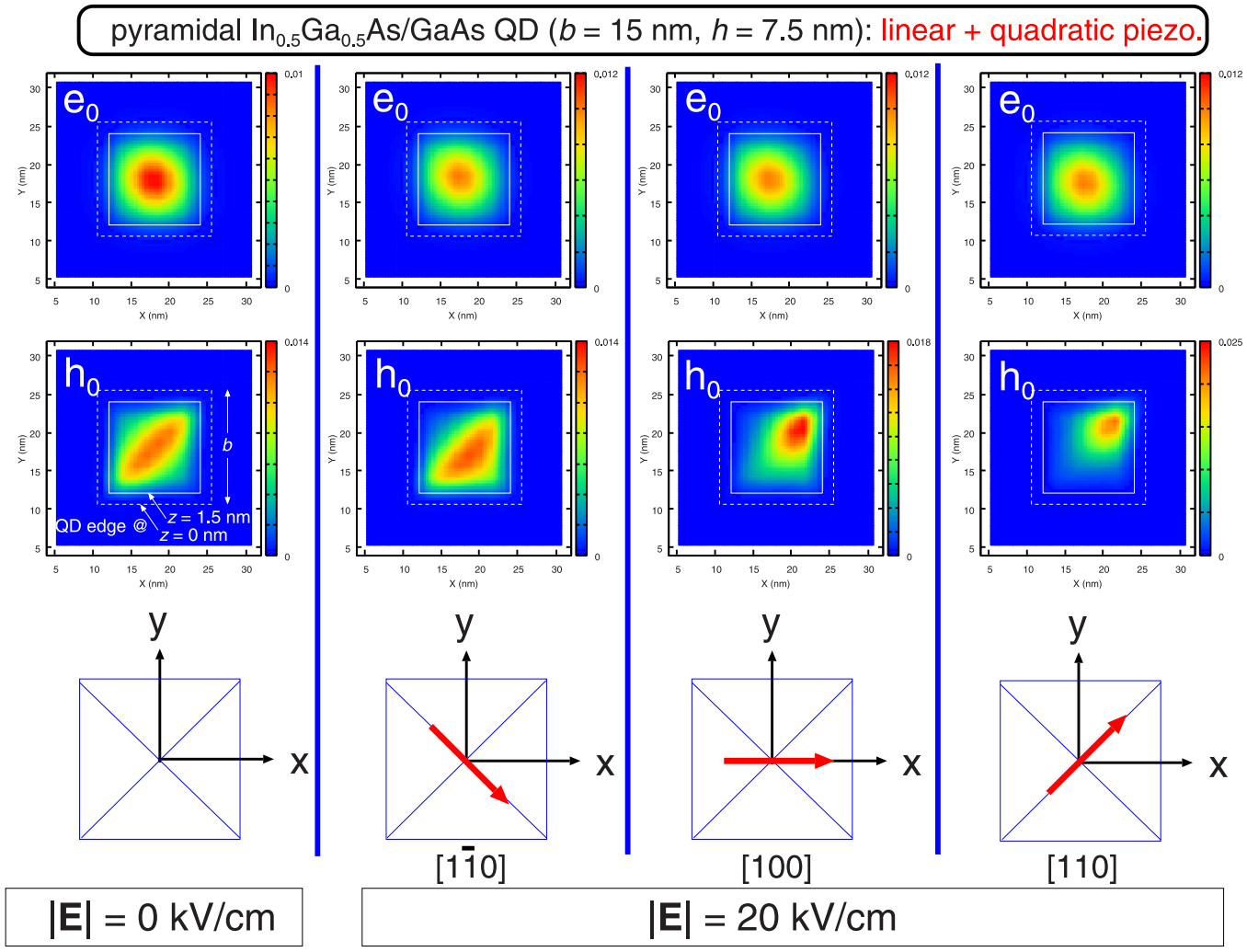

FIG. 6. (Color online) Squared envelope functions, $|\mathbf{F}|^2$, for ground-state electron e_0 and hole h_0 in the pyramidal $In_{0.5}Ga_{0.5}As/GaAs$ quantum dot (the base length $b = 15$ nm) under the lateral electric fields $\mathbf{E}$: $|\mathbf{E}| = 0$ kV/cm and $|\mathbf{E}| = 20$ kV/cm with $\mathbf{E} \parallel [1\bar{1}0]$, $\mathbf{E} \parallel [100]$, and $\mathbf{E} \parallel [110]$ (from left to right). In each panel, the upper plot is for e_0 and the lower one is for h_0. $|\mathbf{F}|^2$ on a (001) plane at $z = 1.5$ nm is displayed; here the quantum dot base is at $z = 0$ nm. The linear and quadratic piezoelectricity is included in the calculation.

For e_0, changes of $|\mathbf{F}|^2$ are inappreciable for the three field directions examined, $[1\bar{1}0]$, [100], and [110], because of the lighter effective mass of the electron. The dependence of $|\mathbf{F}|^2$ for h_0 on the lateral field direction eventually causes the dependence of the excitonic transition energies on the field direction as described later in Fig. 10.

Figure 7 shows $|\mathbf{F}|^2$ for h_0 on the same (001) plane under $|\mathbf{E}| = 0$ kV/cm and $|\mathbf{E}| = 20$ kV/cm with the three field directions examined above, where $|\mathbf{F}|^2$ is calculated with the linear piezoelectricity only (the upper plots) or the quadratic one only (the lower plots). Under $|\mathbf{E}| = 0$ kV/cm, the elongation direction of $|\mathbf{F}|^2$ for the linear-only case differs by 90 degrees from that for the quadratic-only case, since the sign of V_p for the former case is opposite to that for the latter case as already shown in Fig. 5. The symmetries of $|\mathbf{F}|^2$ for the linear-only case with $\mathbf{E} \parallel [1\bar{1}0]$, $\mathbf{E} \parallel [100]$, and $\mathbf{E} \parallel [110]$ are equivalent to those for the quadratic-only case with $\mathbf{E} \parallel [110]$, $\mathbf{E} \parallel [100]$, and $\mathbf{E} \parallel [1\bar{1}0]$, respectively, *after a rotation of* 90 *degrees*. This equivalence comes from the fact that the angle between the $|\mathbf{F}|^2$ elongation direction under $|\mathbf{E}| = 0$ kV/cm and the field direction is 90 degrees, 45 degrees, and 0 degrees, respectively, in the above sequence of the field for both linear- and quadratic-only cases. On the other hand, $|\mathbf{F}|^2$ is much more localized for the linear-only case than for the quadratic-only case.

$|\mathbf{F}|^2$ for h_0 calculated with both linear and quadratic piezoelectricity (the lower plots in Fig. 6) and that calculated with the linear piezoelectricity only (the upper plots in Fig. 7) are almost similar in symmetry. The only quantitative difference is that $|\mathbf{F}|^2$ is somewhat more localized for the latter than for the former. (For example, under $|\mathbf{E}| = 0$ kV/cm, the latter is more localized near the QD corners on the [110] diagonal.) This is because the total V_p is largely dominated by the linear piezoelectric contribution as already shown in Fig. 5.

C. Envelope functions calculated with no piezoelectricity

In order to clarify an effect of the piezoelectricity on the excitonic transition energies ω, we perform the calcultions with no piezoelectricity.

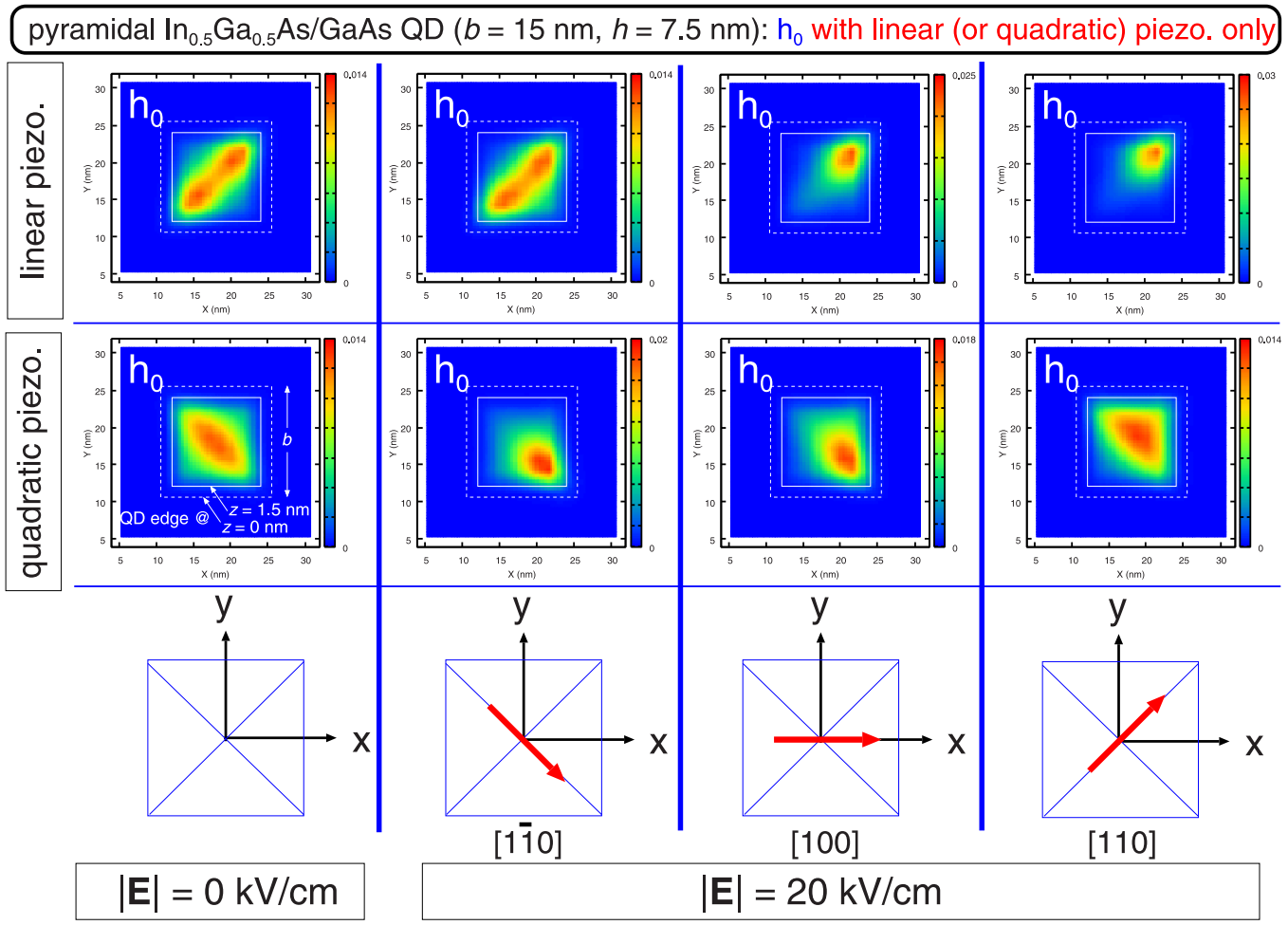

FIG. 7. (Color online) Squared envelope functions, $|\mathbf{F}|^2$, for the ground-state hole h_0 in the pyramidal $In_{0.5}Ga_{0.5}As/GaAs$ quantum dot (the base length $b = 15$ nm) under lateral electric fields $\mathbf{E}$: $|\mathbf{E}| = 0$ kV/cm and $|\mathbf{E}| = 20$ kV/cm with $\mathbf{E} \parallel [1\bar{1}0]$, $\mathbf{E} \parallel [100]$, and $\mathbf{E} \parallel [110]$ (from left to right). In each panel, the upper plot is calculated with the linear piezoelectricity only, and the lower one is calculated with the quadratic piezoelectricity only. $|\mathbf{F}|^2$ on a (001) plane at $z = 1.5$ nm is displayed; here the quantum dot base is at $z = 0$ nm.

Figure 8 shows $|\mathbf{F}|^2$ on the same (001) plane as in Fig. 6 for e_0 and h_0 under $|\mathbf{E}| = 0$ kV/cm and $|\mathbf{E}| = 20$ kV/cm with $\mathbf{E} \parallel [1\bar{1}0]$, [100], and [110], where no piezoelectricity is included in the calculation, putting $V_p = 0$. Under $|\mathbf{E}| = 0$ kV/cm, $|\mathbf{F}|^2$ for h_0 shows C_{4v} symmetry due to the absence of the piezoelectric potential V_p having C_{2v} symmetry [Fig. 5(c)].

With $\mathbf{E} \parallel [1\bar{1}0]$ and $\mathbf{E} \parallel [110]$, $|\mathbf{F}|^2$'s for h_0 are deviated toward the QD corners in the $[1\bar{1}0]$ and [110] directions, respectively, following the field directions. Both $|\mathbf{F}|^2$'s have C_{1v} symmetry. $|\mathbf{F}|^2$ for h_0 with $\mathbf{E} \parallel [1\bar{1}0]$ is identical to that with $\mathbf{E} \parallel [110]$ by a rotation of 90 degrees around the z axis. This is a result different from that in the calculation including the piezoelectricity where both $|\mathbf{F}|^2$'s are considerably different as shown in Fig. 6.

With $\mathbf{E} \parallel [100]$, $|\mathbf{F}|^2$ for h_0 moves toward the QD edge in the [100] direction showing the C_{1v} symmetry, while the corresponding $|\mathbf{F}|^2$ calculated with the piezoelectricity moves toward the QD corner in the [110] direction.

For the three field directions, the change in extent of $|\mathbf{F}|^2$ for h_0 is not remarkable in the calculation with no piezoelectricity, while the change is remarkable in that with the piezoelectricity. *This demonstrates that the piezoelectricity causes the strong dependence of $|\mathbf{F}|^2$ for h_0 on the field direction.*

For e_0, changes of $|\mathbf{F}|^2$ are inappreciable for the three field directions as in the calculation with the piezoelectricity.

D. Coulomb energies and transition energies

Figure 9 shows the single-particle energy difference $(e_0 - h_0)$ and Coulomb energies $[J(e_0h_0)$, $J(h_0h_0)$, and $J(e_0e_0)]$ under $|\mathbf{E}| = 0$ kV/cm and $|\mathbf{E}| = 20$ kV/cm with $\mathbf{E} \parallel [1\bar{1}0]$, [100], and [110], which are calculated including (a) the linear and quadratic piezoelectricity and (b) no piezoelectricity. The energy difference $(e_0 - h_0)$ under $|\mathbf{E}| = 20$ kV/cm shows redshifts of the QCSE. $(e_0 - h_0)$ calculated with the piezoelectricity decreases with variation of the field direction as $[1\bar{1}0] \rightarrow [100] \rightarrow [110]$, while that calculated with no piezoelectricity shows an inappreciable direction dependence. At the same time, $|J(e_0h_0)|$ and $J(h_0h_0)$ calculated with the piezoelectricity decreases and increases, respectively, with variation of the field direction as above, while those calculated with no piezoelectricity again show an inappreciable direction

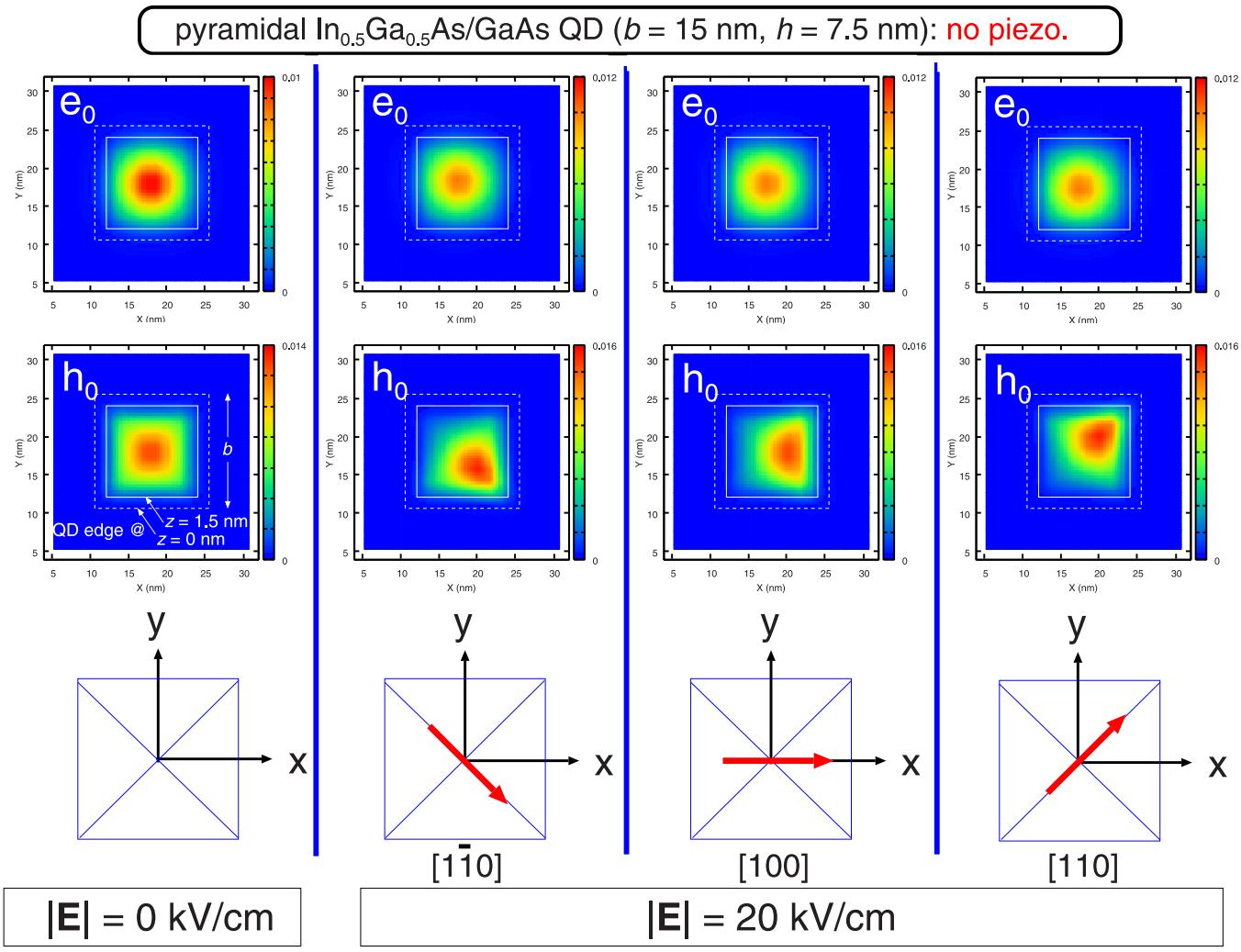

FIG. 8. (Color online) Identical to Fig. 6, but no piezoelectricity is included in the calculation.

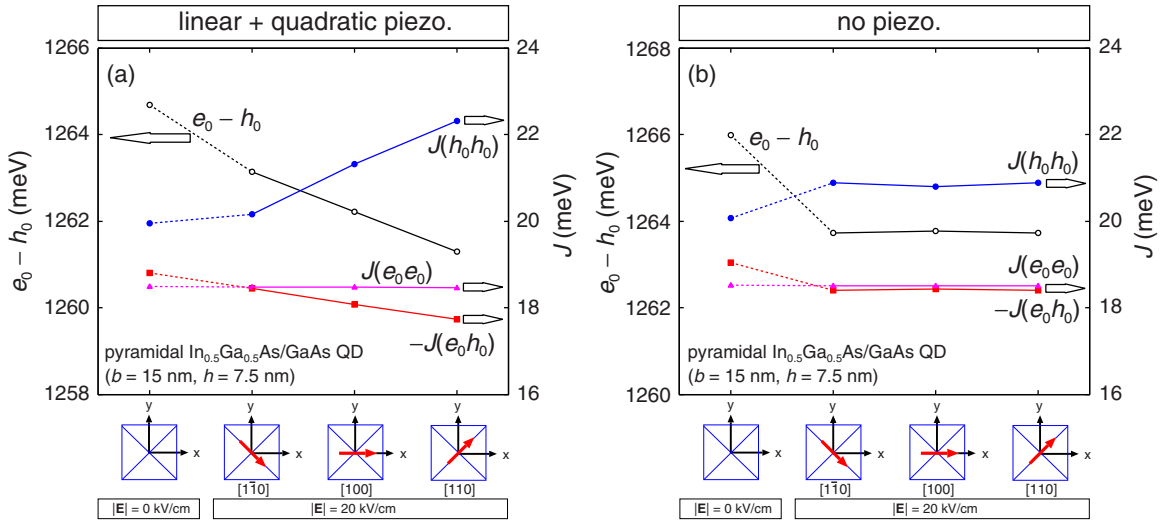

FIG. 9. (Color online) Single-particle energy difference $(e_0 - h_0)$ and electron-hole, hole-hole, and electron-electron Coulomb energies $[J(e_0h_0)$, $J(h_0h_0)$, and $J(e_0e_0)$, respectively] in the pyramidal $In_{0.5}Ga_{0.5}As/GaAs$ quantum dot (the base length $b = 15$ nm) under lateral electric fields $\mathbf{E}$: $|\mathbf{E}| = 0$ kV/cm and $|\mathbf{E}| = 20$ kV/cm with $\mathbf{E} \parallel [1\bar{1}0]$, $\mathbf{E} \parallel [100]$, and $\mathbf{E} \parallel [110]$. In the calculation, we include (a) the linear and quadratic piezoelectricity and (b) no piezoelectricity. In both figures, the left vertical axis is for $e_0 - h_0$ and the right one is for J's. Note that the sign is reversed for $J(e_0h_0)$.

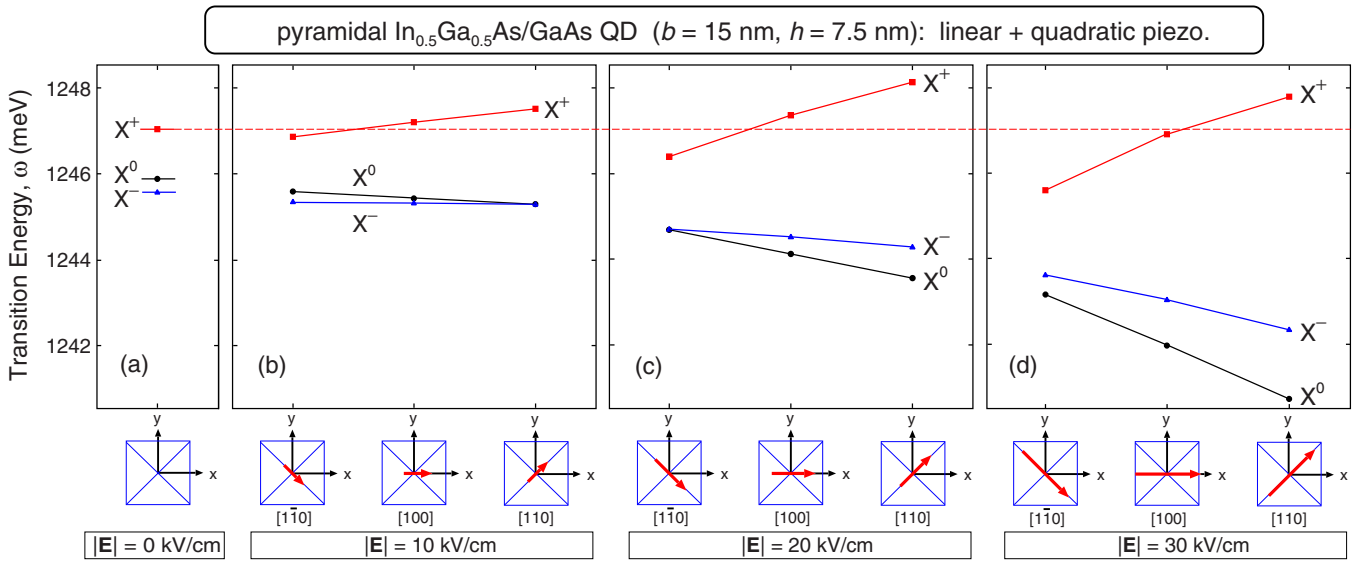

FIG. 10. (Color online) Transition energies ω for neutral excitons (X^0) and positively and negatively charged excitons (X^+ and X^-, respectively) in the pyramidal $In_{0.5}Ga_{0.5}As/GaAs$ quantum dot (the base length $b = 15$ nm) under lateral electric fields $\mathbf{E}$: $|\mathbf{E}|$ = (a) 0 kV/cm, (b) 10 kV/cm, (c) 20 kV/cm, and (d) 30 kV/cm. The field directions are $\mathbf{E} \parallel [1\bar{1}0]$, $\mathbf{E} \parallel [100]$, and $\mathbf{E} \parallel [110]$. The horizontal dashed line indicates $\omega(X^+)$ at $|\mathbf{E}| = 0$ kV/cm. The linear and quadratic piezoelectricity is included in the calculation.

dependence. $J(e_0e_0)$ shows little direction dependence with and without the piezoelectricity.

In the presence of the piezoelectricity, the direction dependence of $|J(e_0h_0)|$ and $J(h_0h_0)$ originates from that of $|\mathbf{F}|^2$ for h_0 as already shown in Fig. 6. With variation of the field direction as $[1\bar{1}0] \rightarrow [100] \rightarrow [110]$, the extent of $|\mathbf{F}|^2$ for h_0 decreases. As a result, $|J(e_0h_0)|$ decreases due to the reduction of overlap between e_0 and h_0 wave functions, and $J(h_0h_0)$ increases due to the enhancement of the hole density.

Using the values $(e_0 - h_0)$ and Coulomb energies in Fig. 9, we calculate the excitonic transition energies ω, including linear and quadratic piezoelectricity (Fig. 10) and not including piezoelectricity (Fig. 11). Here the field strengths $|\mathbf{E}|$ of 10 and 30 kV/cm are examined in addition to 20 kV/cm. With the piezoelectricity (Fig. 10), $\omega(X^0)$ and $\omega(X^-)$ show direction-dependent redshifts under the field strength examined: both ω's decrease with variation of the field direction as $[1\bar{1}0] \rightarrow [100] \rightarrow [110]$. We also find that X^- is binding under $|\mathbf{E}| = 10$ kV/cm, while it is antibinding under $|\mathbf{E}| = 20$ and 30 kV/cm. $\omega(X^+)$ shows a more remarkable direction-dependence: a redshift with $\mathbf{E} \parallel [1\bar{1}0]$ and unusual blueshifts with $\mathbf{E} \parallel [100]$ and [110] under $|\mathbf{E}| = 10$ and 20 kV/cm. (Under $|\mathbf{E}| = 30$ kV/cm, a blueshift occurs only with $\mathbf{E} \parallel$ [110].) As a whole, the direction dependence of $\omega(X^0)$, $\omega(X^-)$, and $\omega(X^+)$ is larger for higher field strength.

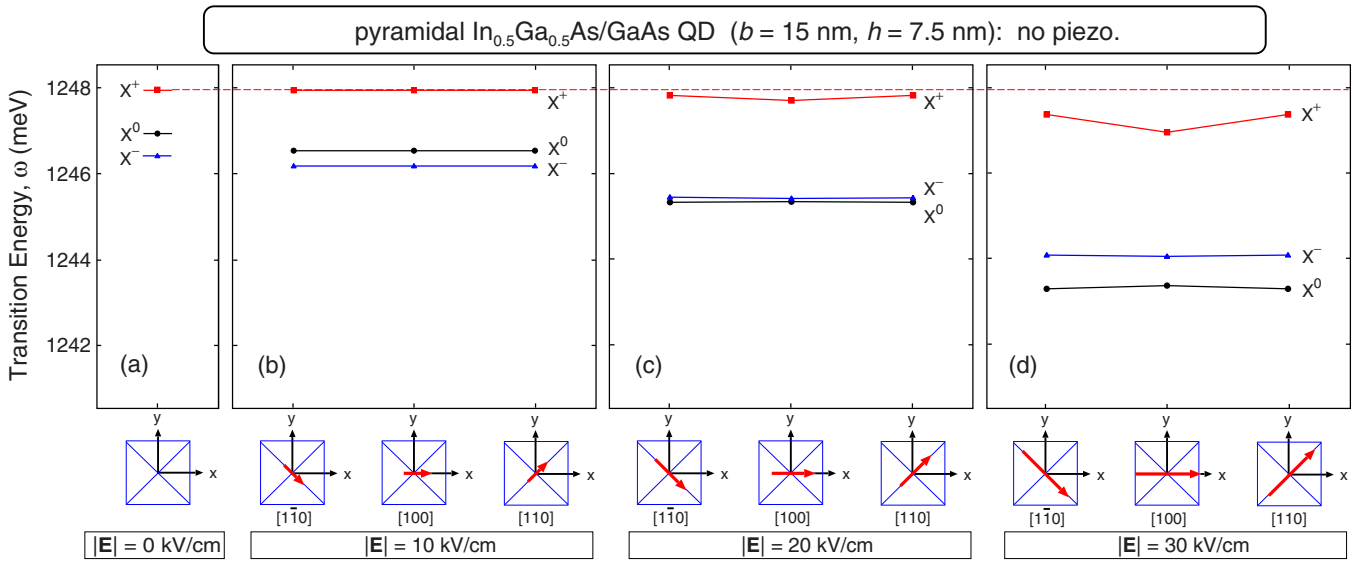

FIG. 11. (Color online) Identical to Fig. 10, but no piezoelectricity is included.

In contrast, the transition energies calculated with no piezoelectricity (Fig. 11) show *only redshifts* with inappreciable direction dependence, except that $\omega(X^+)$ under $|\mathbf{E}| = 30$ kV/cm shows some direction dependence.

By comparing Figs. 9, 10, and 11, it is clearly understood that the direction-dependent ω's calculated with the piezoelectricity are a result of the direction dependence of the Coulomb energies, $J(e_0h_0)$ and $J(h_0h_0)$.

V. CONCLUSIONS

We have calculated the excitonic transition energies [$\omega(X^0)$, $\omega(X^+)$, $\omega(X^-)$] in pyramidal $In_{0.5}Ga_{0.5}As$/GaAs QDs under a lateral electric field $\mathbf{E}$ up to 40 kV/cm. First, the single-particle electron and hole states under the lateral field are calculated using the 8-band $\mathbf{k}\cdot\mathbf{p}$ theory. The linear and quadratic piezoelectricity is included. Next, the transition energies ω are calculated from the Coulomb energies [$J(e_0h_0)$, $J(e_0e_0)$, and $J(h_0h_0)$]. For a QD with 15-nm base length under $\mathbf{E} \parallel [100]$, $\omega(X^+)$ exhibits a blueshift with increasing $|\mathbf{E}|$ up to 28 kV/cm, followed by a redshift under higher $|\mathbf{E}|$. In contrast, $\omega(X^0)$ and $\omega(X^-)$ exhibit only redshifts accompanied by a crossing of the two exciton levels. The calculated result for X^+ reproduces the unconventional "M"-shaped exciton energy shift observed in the experiment by Nakaoka *et al.* [11]. We find that a QD size with 13.75-nm base length is appropriate to reproduce the observed PL blueshift. The origin of the blueshift calculated for X^+ is the enhanced hole density in the QD base corner due to the modification of the piezoelectric potential V_p by the lateral electric field, which causes an increase in the Coulomb energy $J(h_0h_0)$. We find that the amount of the blueshift increases with the QD size. In order to understand the effect of the lateral field *direction*, we calculate the transition energies with $\mathbf{E} \parallel [1\bar{1}0]$, [100], and [110]. Under $|\mathbf{E}| = 10$ and 20 kV/cm, $\omega(X^+)$ exhibits a redshift for the $[1\bar{1}0]$ direction and the blueshifts of different amounts for the [100] and [110] directions, indicating that the effects of the lateral field are not equivalent for the $[1\bar{1}0]$ and [110] directions. It is demonstrated that the direction dependence of the transition energy reflects the symmetry of the confinement potential in the QDs due to the piezoelectricity.

ACKNOWLEDGMENTS

We would like to thank Y. Tamura, T. Miyazawa, K. Watanabe, Y. Ota, and S. Iwamoto for discussions on the experimental data in Ref. [11]. This work was supported by the Project for Developing Innovation Systems of the Ministry of Education, Culture, Sports, Science and Technology (MEXT), Japan.

[1] *Nano-Optoelectronics: Concepts, Physics, and Devices*, edited by M. Grundmann (Springer-Verlag, New York, 2002).
[2] R. J. Young, D. J. P. Ellis, R. M. Stevenson, A. J. Bennett, P. Atkinson, K. Cooper, D. A. Ritchie, and A. J. Shields, Proc. IEEE **95**, 1805 (2007).
[3] P. W. Fry, I. E. Itskevich, D. J. Mowbray, M. S. Skolnick, J. J. Finley, J. A. Barker, E. P. O'Reilly, L. R. Wilson, I. A. Larkin, P. A. Maksym, M. Hopkinson, M. Al-Khafaji, J. P. R. David, A. G. Cullis, G. Hill, and J. C. Clark, Phys. Rev. Lett. **84**, 733 (2000).
[4] R. M. Stevenson, R. J. Young, P. See, D. G. Gevaux, K. Cooper, P. Atkinson, I. Farrer, D. A. Ritchie, and A. J. Shields, Phys. Rev. B **73**, 033306 (2006).
[5] T. Nakaoka, T. Kakitsuka, T. Saito, S. Kako, S. Ishida, M. Nishioka, Y. Yoshikuni, and Y. Arakawa, J. Appl. Phys. **94**, 6812 (2003).
[6] W. Sheng and J.-P. Leburton, Phys. Rev. Lett. **88**, 167401 (2002).
[7] W. Sheng and J.-P. Leburton, Phys. Rev. B **67**, 125308 (2003).
[8] B. D. Gerardot, S. Seidl, P. A. Dalgarno, R. J. Warburton, D. Granados, J. M. Garcia, K. Kowalik, O. Krebs, K. Karrai, A. Badolato, and P. M. Petroff, Appl. Phys. Lett. **90**, 041101 (2007).
[9] M. Kaniber, M. F. Huck, K. Müller, E. C. Clark, F. Troiani, M. Bichler, H. J. Krenner, and J. J. Finley, Nanotechnology **22**, 325202 (2011).
[10] M. E. Reimer, M. P. van Kouwen, A. W. Hidma, M. H. M. van Weert, E. P. A. M. Bakkers, L. P. Kouwenhoven, and V. Zwiller, Nano Lett. **11**, 645 (2011).
[11] T. Nakaoka, Y. Tamura, T. Saito, T. Miyazawa, K. Watanabe, Y. Ota, S. Iwamoto, and Y. Arakawa, Appl. Phys. Lett. **99**, 181109 (2011).
[12] T. B. Bahder, Phys. Rev. B **41**, 11992 (1990).
[13] A. Schliwa, M. Winkelnkemper, and D. Bimberg, Phys. Rev. B **79**, 075443 (2009).
[14] S. Ritter, P. Gartner, N. Baer, and F. Jahnke, Phys. Rev. B **76**, 165302 (2007).
[15] M. Korkusinski, M. E. Reimer, R. L. Williams, and P. Hawrylak, Phys. Rev. B **79**, 035309 (2009).
[16] G. Bester, A. Zunger, X. Wu, and D. Vanderbilt, Phys. Rev. B **74**, 081305(R) (2006).
[17] A. Schliwa, M. Winkelnkemper, and D. Bimberg, Phys. Rev. B **76**, 205324 (2007).
[18] T. Nakaoka, T. Saito, J. Tatebayashi, and Y. Arakawa, Phys. Rev. B **70**, 235337 (2004).
[19] M. Grundmann, O. Stier, and D. Bimberg, Phys. Rev. B **52**, 11969 (1995).
[20] F. Boxberg and J. Tulkki, Rep. Prog. Phys. **70**, 1425 (2007).
[21] T. Saito, H. Ebe, Y. Arakawa, T. Kakitsuka, and M. Sugawara, Phys. Rev. B **77**, 195318 (2008).
[22] W. Sheng and J.-P. Leburton, Phys. Rev. B **64**, 153302 (2001).
[23] S. Rodt, A. Schliwa, K. Pötschke, F. Guffarth, and D. Bimberg, Phys. Rev. B **71**, 155325 (2005).
[24] F. Guffarth, R. Heitz, A. Schliwa, O. Stier, M. Geller, C. M. A. Kapteyn, R. Sellin, and D. Bimberg, Phys. Rev. B **67**, 235304 (2003).